Journal of
Renewable Energy Research and Applications (RERA)

Published online

Simulation Study of Cs_2TiBr_6 Perovskite Solar Cells Using Graphene Oxide as a Novel HTL Layer Using SCAPS 1-D

T. Titu

Nirmala College Muvattupuzha, Kerala, India.

Received Date 02 August 2022; Revised Date 05 September 2022; Accepted Date 26 September 2022
**Corresponding author: tt@nirmalacollege.ac.in (T. Titu)*

Abstract

Highly unstable absorber layers along with costly Hole Transport Materials (HTMs) have been the main problems in the perovskite-based photovoltaic industry recently. Here, in this work, we intend to meet both of these problems by introducing a non-toxic caesium-based absorber layer and low-cost material, Graphene Oxide (GO), as the Hole Transporting Layer (HTL). We use the Solar Cell Capacitance Simulator (SCAPS) program to study the various output parameters of the device with the structure GO/Cs_2TiBr_6/TiO_2. The physical properties like the thickness of the absorber and hole transporting layers, the role of the layer interfaces, the effect of electron affinity, optical properties like the band gap of the absorber and hole transporting layer, electrical properties like the parasitic resistance, and finally, the influence of operating conditions like the temperature on the working of the device are found out. The results obtained show that a thickness of 1 μm for absorber and 0.1 μm for HTL is suitable. Also the optimum values for the front and back interface layers are 10^{10} cm^{-3} and 10^{16} cm^{-3}, respectively. The resistance values are fixed at 2Ω for the series, and 40Ω for the shunt resistance. The electron affinity does not seem to have much effect on the device performance, while with the increase in the temperature, the performance of the device deteriorates. The highest efficiency that we obtain from the optimized device is 15.3%. In short, this unprecedented work shows that the Cs_2TiBr_6-GO-based devices are suitable candidates to achieve highly efficient, eco-friendly, all-inorganic perovskite solar cells.

Keywords: *Perovskites, SCAPS, Graphene Oxide, Cs_2TiBr_6, Numerical Simulation.*

1. Introduction

Solar energy is the ultimate answer to the critical energy scenario that we are facing today. It also paves the path toward a green and clean energy. As of today, silicon solar cells in grids contribute a major portion of the solar energy harvesting systems [1]. A lot of work is being carried out around the globe to increase the efficiency of the device, and a maximum of 47% has already been attained [2]. Along with silicon solar cells, various organic-inorganic materials [3] are also at the front of photovoltaic device research [4], [5]. Recently, perovskite solar cells (PSCs) have gained much importance in the photovoltaic world due to their attractive characteristics like tuneable band gap [6], [7], high absorption coefficient [8], high carrier mobility [9], low exciton binding energy, long diffusion length [10], etc. The efficiency of perovskite solar cells have jumped from 3.8% to 25% in a surprisingly short span of time [11].

Despite its huge advantages, perovskite solar cells are not free of drawbacks [12], [13]. Generally, an organic-inorganic perovskite belongs to a class of materials with the formula XYZ_3, where X and Y are cations and Z any halogen anion [14], [15]. Some of the common X cations like CH_3NH_3, Formabidinium etc.

[16], [17] create instability due to their enormous polar nature, and thereby, reducing the shelf life of the device [18], [19]. On the other side, the most commonly used Y cations such as Pb and Sn are toxic and raise concerns about their use at the commercial level [20], [21]. Thus efforts are being made to develop novel materials that overcome these shortcomings, and have the same performance level as the already established perovskites has [22]. The stability issue can be addressed by replacing the organic ion with any inorganic ion such as Cs and Ge [23], [24]. Among them, inorganic Caesium-based perovskites have attracted more attention recently

due to the high stability and mobility of charge carriers [25] as compared to their competitors. Caesium also possesses the tolerance factor [26] to maintain the perovskite structure, restricting any phase change, has a better light absorption, and can be easily doped with existing perovskites without disrupting the crystal structure due to its lower ionic radius [27]. However, the caesium-based perovskite family $CsPbX_3$, where X is any halogen still possessing the drawback of Pb toxicity limiting its usage. Ju et al. have introduced a lead-free caesium titanium halide family with a double perovskite structure [28] (Cs_2TiX_6, X=Br, I, F, Cl)[29] having an adjustable band gap, thermal stability, room temperature fabrication process [30], and most importantly, removing the problem of Pb toxicity making them an ideal absorber layers in the perovskite solar structures. Later, Chen et al. developed a Cs_2TiBr_6 thin film as a novel absorber layer with an efficiency of 3% and showing superior stability to methylammonium and formabidinium absorber layers [31].

Hole Transporting Layer (HTL) and Electron Transport Layer (ETL) also play a vital role in the performance of perovskite solar cells [32], [33]. Suitable HTLs and ETLs act as a path for the carriers to reach the respective electrodes [34], [35]. Most often, hole transporting layers are generally organic polymers such as [2,2',7,7'-Tetrakis[N,N-di(4-methoxyphenyl)amino]-9,9'-spirobifluorene] (Spiro-OMeTAD)[36], poly(triaryl amine) (PTAA)[37], poly(3-hexylthiophene-2,5-diyl) (P3HT) [38], and poly(3,4-ethylenedioxythiophene): poly(styrene sulfonate) (PEDOT: PSS) [39], etc. [40], [41]; most of these HTL materials are very expensive; at the same time, they are highly unstable. Recently, graphene and its derivatives like graphene oxide and reduced graphene oxide have started to revolutionize the optoelectronic industry with its unique properties [42], [43]. In this work, we introduce Graphene Oxide (GO) as a novel hole transporting material. Graphene oxide has already been reported as a front electrode and hole transporting layer in various perovskite structures. They have reduced the stability of the perovskite devices due to moisture, ion electromigration, temperature, etc. Graphene oxide in the form of quantum dots has been used in perovskite solar cells, and increases the efficiency of the device [44]. They are also used in nanocomposite forms as they have low processing costs and large-scale development possibility.

Here, in this work, we introduce the device structure FTO/GO/Cs_2TiBr_6/TiO_2. The main purpose of the work is to find the feasibility of using graphene oxide as an effective HTL along with the Cs_2TiBr_6 absorber layer. Different influencing parameters are varied thoroughly to study the effects on the photovoltaic parameters such as the open circuit voltage, short circuit current, fill factor, and the efficiency of the device.

2. Methodology

Numerical simulation is a crucial part of any experiment saving a vast amount of time, and cost and giving a deep insight into the actual physical phenomenon playing inside. There are many simulation packages available in the market such as COMSOLE, MATLAB, and SCAPS-1D, AMPS. Here, we use the SCAPS (Solar Cell Capacitance Simulator) software developed at the Department of Electronics and Information System, University of Gent, Belgium [45]. The program uses the three equations the carrier continuity equations, the poisons equation, and the drift–diffusion equation (1-7), and solves these equations for various input parameters to give various device outputs [46], [47].

$$\frac{\partial^2 \varphi}{\partial x^2} = \frac{q}{\varepsilon}(n - p) \tag{1}$$

$$\frac{\partial n}{\partial t} = \frac{1}{q}\frac{\partial j_n}{\partial x} + (G - R) \tag{2}$$

$$\frac{\partial p}{\partial t} = -\frac{1}{q}\frac{\partial j_p}{\partial x} + (G - R) \tag{3}$$

$$J_n = qD_n\frac{\partial n}{\partial x} - q\mu_n n\frac{\partial \varphi}{\partial x} \tag{4}$$

$$J_p = -qD_p\frac{\partial p}{\partial x} - q\mu_p p\frac{\partial \varphi}{\partial x} \tag{5}$$

where ϕ is the electric potential, q is the electronic charge, ε is the dielectric constant, n is the electron concentration, p is the hole concentration, J_n is the electron density, J_p is the hole current density, G is the carrier generation rate, and R is the carrier recombination rate. D_n and D_p are the electron and hole diffusion coefficients, respectively, and μ_n and μ_p are the electron and hole mobility, respectively.

The solar cell capacitance simulator is preferable to other simulation packages due to its user-friendly interface and flexibility in setting various parameters. Also the results are available in a wide variety of formats including current-voltage, capacitance-voltage, quantum efficiency, band structures, recombination rates, etc. [48]. On the other hand, the users can easily vary the different parameters that affect the performance of the

devices. The materialistic properties like the thickness, band gap, electron affinity, carrier concentration, and other operating parameters like the temperature, applied voltage, frequency, and illumination can all be changed easily. The device is represented as a stack of different layers in the software, and any device with up to 7 layers can be simulated using SCAPS 1-D. Along with that, there are also provisions for front and back contacts, and to determine the effect of various interfaces between these layers [28]. All these properties can be varied to obtain the output parameters both in the dark and illuminated conditions.

3. Device structure and simulation parameters

As mentioned earlier, the proposed device has a structure FTO/TiO_2/ Cs_2TiBr_6/GO/Metal Contact. Table 1 gives the simulation parameters that we have used in the article. Also table 2 shows the defect density parameters used in the model. The values are taken from various published articles and a few by reasonable assumption. Band alignment is very important in the case of charge diffusion of heterojunction solar cells, and the band alignment diagram is given in figure 1. The simulation is conducted under the illumination of AM1.5G with an intensity of 1000 mW/cm^2 at the 300 K operating temperature. In this work, the properties like thickness, bandgap, electron affinity, and doping density are studied. Two interfacial layers Cs_2TiBr_6/TiO_2 and Cs_2TiBr_6/GO are also studied on their interfacial defects. Finally, the influence of the series and shunt resistance and operating temperature on their device performance was also studied.

Table 1. Simulation parameters for each layer of the proposed PSC.

Properties	Tio_2	Cs_2TiBr_6	GO
Thickness	232	200	100
Bandgap	3.2	1.8	2.48
Electron affinity	4.1	4.0	2.3
Dielectric permittivity (relative)	9	10	10
Conduction band effective density of states	2.2E+18	6E + 19	2.2E+18
Valence band effective density of states	1E+19	2.14E+19	1.8E+19
Electron mobility	20	0.236	26
Hole mobility	10	0.171	123
Donor density	1E+18	3E+19	0
Acceptor density	0	3E+18	2.0E+18
References	[49]	[50]	[51]

Table 2. Parameters setting of interface defects.

Defect type	Neutral
Defect density	10^{15}
Electron capture cross section	10^{-17}
Hole capture cross section	10^{-18}
Distribution	Gaussian
Defect energy level with respect to reference	At the middle of band gap
Characteristic energy (eV)	1.1

General parameters used in defect layers

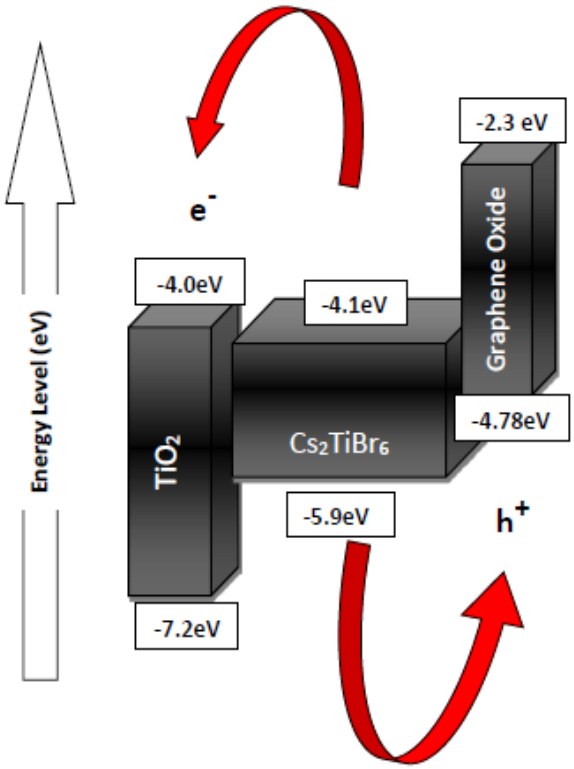

Figure 1. Energy band information of the device.

3. Results and Discussion

Absorber layer thickness variation

In a perovskite solar cell, the most important portion is the perovskite layer since it is where the solar energy is absorbed. The thickness of this layer hence decides the efficiency of the device. In this work, the influence of the absorber layer was examined by varying the thickness of the absorber layer from 0.01 µm to 1 µm. Figure 2 shows in detail the variation of photovoltaic parameters with the change in the absorber thickness. It is seen that all the photovoltaic parameters are enhanced. The efficiency of the device increased from 4.2% at 0.1 µm to 10.2% at 1 µm thickness of the Cs_2TiBr_6 layer, and this increase in efficiency can be attributed due to the increase in short circuit current from 10.2 mAcm^{-2} to 23.47 mAcm^{-2}. This directly implies an increase in charge carriers with the increase in thickness.

To further study this phenomenon, the Quantum Efficiency (QE) of the device was noted along with the absorber thickness. Quantum efficiency gives information about how well the carriers are generated from the incident photons of a particular wavelength. Figure 3 shows the variation of QE with the wavelength of the proposed device with different absorber thicknesses. It can be seen that with the increase in absorber thickness, the QE of the device increases in the longer wavelength region. This is

expected since with the increase in absorber thickness, more photon-generated electron-hole pairs will be generated. Also for incident light above 800 nm, QE was reduced to zero implying the mismatch between incoming photon energy and the bandgap of the absorber material. It is also noted that the parameters go to saturation when the thickness reaches about 1 μm. Fill factor and V_{oc} levels are at almost 78% and 0.55 V, respectively. This is due to the recombination of the charge carriers within the thick absorber layer before reaching the electrodes or theoretically, then the thickness of the layer will be greater than the diffusion length of the carriers. Thuis the optimum thickness of the absorber layer is taken at 1 μm for further study.

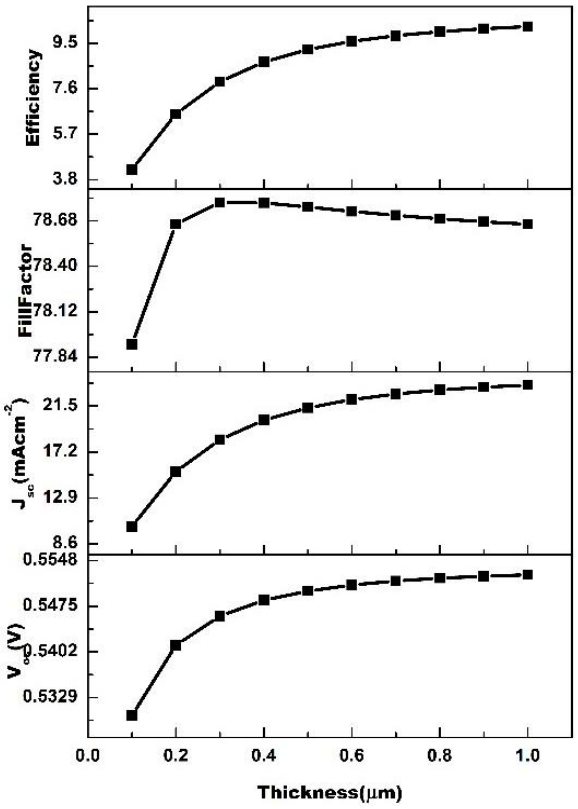

Figure 2. Variation in photovoltaic parameters with absorber layer thickness.

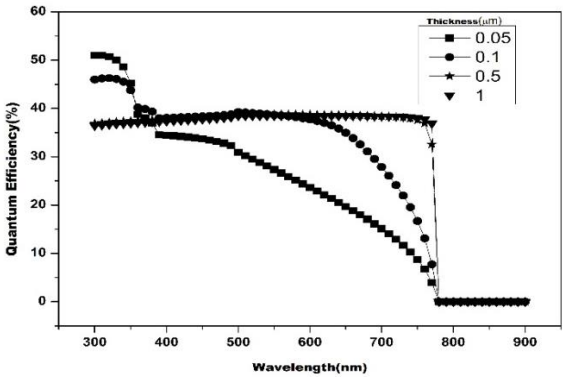

Figure 3. Quantum efficiency study of the device with variation in absorber layer thickness.

HTL layer thickness variation

The HTL generally blocks the electrons, and provides a suitable passage for the photogenerated holes to reach the electrodes without any short circuit in between [52]. Hence, they play a vital role in increasing the efficiency of the device. The HTLs require specific properties like suitable bandgap, work function, and proper thickness. In this work, we have used a novel material, graphene oxide, as the HTL. Figure 4 shows the variation in parameters with HTL thickness. Although the fill factor decreases with the decrease in thickness of the HTL, other parameters increase. J_{sc} decreased slightly from 15 mAcm^{-2} at 0.1 μm to 12.70 mAcm^{-2} at 1 μm. This indicates the loss of charge carriers with an increase in thickness. Increased HTL thickness increases the diffusion length of the charge carriers, and thus the carriers have to travel more distance to reach the counter electrode, thereby decreasing the probability of recombination. The results indicate that graphene oxide used as a thin layer is an effective HTL layer with caesium-based perovskite solar cells.

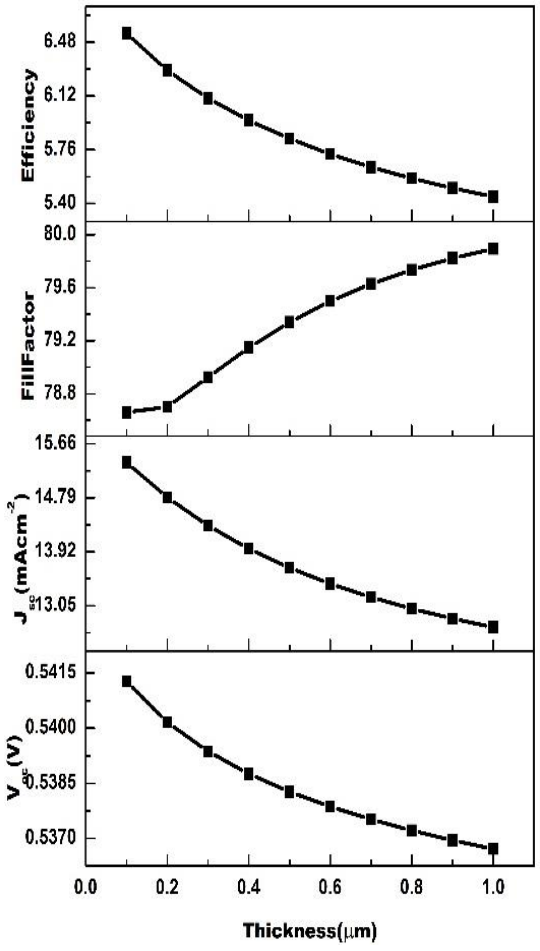

Figure 4. Variation in photovoltaic parameters with thickness of graphene oxide layer.

Interface defect density variations

The interface between the layers in general plays a very crucial role in the performance of the device. If the interface has greater defects, greater will the recombination and loss of carriers, and thereby, decreasing the efficiency of the device. The influence of the interface defects [53] can be seen in equation (6).

$$\boldsymbol{V_{oc} = \frac{1}{q}\{\phi_c + AKTln\left(\frac{qN_vS_{it}}{J_{sc}}\right)\}} \quad (6)$$

where S_{it} is the interface recombination velocity, A is the ideality factor, and Φ_c is the effective barrier height. High interface defects will lead to a low V_{oc}. Here, we have varied the defect densities of both the front and back interfaces, i.e. TiO_2-Cs_2TiBr_6 interface and the back interface Cs_2TiBr_6-GO. The TiO_2-Perovskite interface defect density is varied from 10^{16} cm^{-3} to 10^{20} cm^{-3}, and the back interface between Perovskite- GO varied from 10^{10} cm^{-3} to 10^{15} cm^{-3}. The results obtained are indicated in figures 5a and 5b. All the photovoltaic parameters declined rapidly with the increase in defect density. The parameters decreased drastically till the defect density became 10^{18} cm^{-3}, and then it remained the same. Both the results indicate that the defect density influences the recombination rates, lifetime, and mobility of carriers. With the increase in defect density, the recombination of carriers also increases owing to the decrease in various parameters. The front interface density should be less than 10^{16} cm^{-3} and the back interface density less than 10^{10} cm^{-3}.

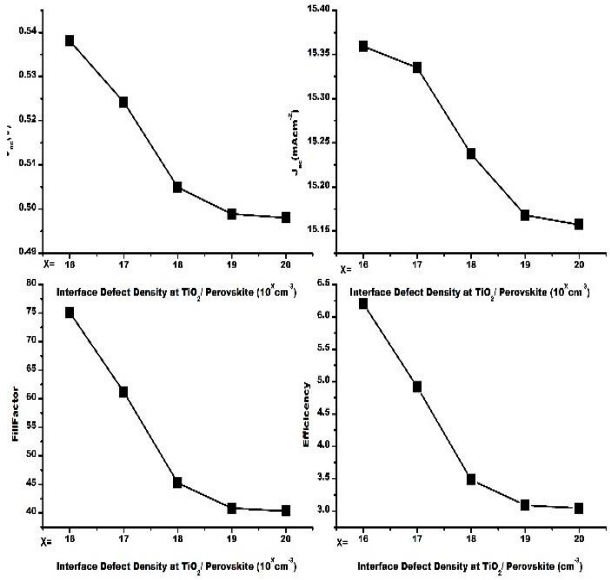

Figure 5(a). Variation in V_{oc}, J_{SC}, FF, and efficiency with variation in defect density at TiO_2/absorber interface.

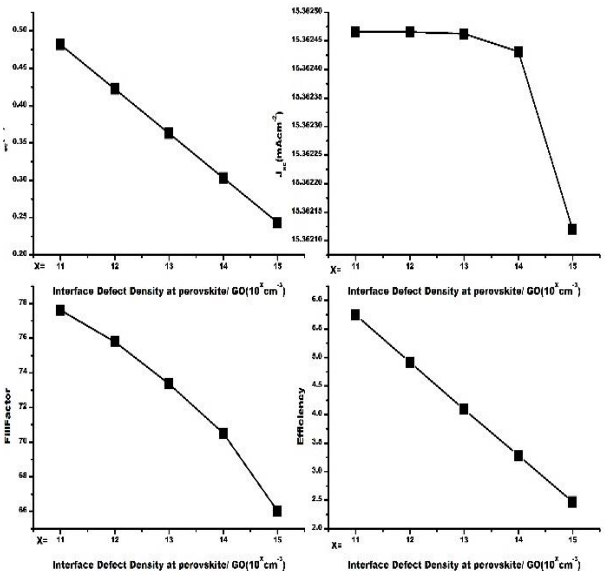

Figure 5(b). Variation in photovoltaic parameters with variation in defect density at absorber/GO interface.

Variation in band GAP of absorber layer

The absorber material Cs_2TiBr_6 is a member of caesium-based perovskites having a general equation Cs_2TiX_6; X is Br, Cl, I or F. All of these members have almost identical properties except bandgap. Their band gap varies from 1.6 eV, 1.8 eV, 1.9 eV, and 2 eV for X as Br, I, F, and Cl, respectively. Here, the bandgap of the absorber material was varied from 1 eV to 2 eV to simulate other members of the same caesium-based perovskite family. From figure 6, it is clear that with the increase in the bandgap of the absorber material, the efficiency decreases drastically from 15% to 3%. This is expected since a higher bandgap for the window layer and a lower bandgap for the absorber layer produce more photogenerated current, and thus increasing FF, and vice versa.

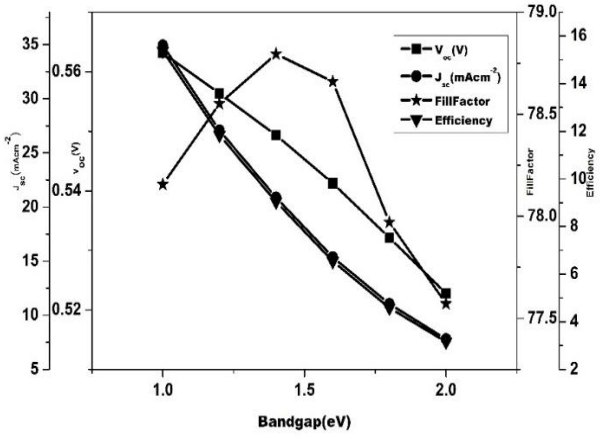

Figure 6. Variation in various photovoltaic parameters with variation in band gap of absorber layer.

Variation in shunt resistance and series resistance

The various internal resistances have a great impact on the performance of the device. The resistance between the different layers of the cell and between the layer and metal contacts are all important factors. The relationship between various parameters of a solar cell can be find out by assuming the diode equivalent model of a solar cell, and based on this and various numerical simulations, a balanced model for a highly efficient perovskite solar cell can be represented as the following equation [54]:

$$\mathbf{J} = \frac{(\boldsymbol{V} - \boldsymbol{JR_s})}{\boldsymbol{R_{sh}}} + \boldsymbol{J_r}(\boldsymbol{V} - \boldsymbol{JR_s}) + \boldsymbol{J_n}(\boldsymbol{V} - \boldsymbol{JR_s}) - \boldsymbol{J_p} \qquad (7)$$

where R_s and R_{sh} refer to series resistance and shunt resistance, J_n and J_r are the current losses due to radiative emission and non-radiative recombination's, and is denoted as the photocurrent obtained by solving the Maxwell's equations. Among the various parameters in his equation for efficiency loss, the most important parameters are the series and shunt resistances. Not only the efficiency, the fill factor of the device also depends on the series and shunt resistance; the fill factor in the presence of series resistance and shunt resistance `is given as equations (8) and (9) [54]:

$$\boldsymbol{FF_s} = \boldsymbol{FF_o}(\mathbf{1} - \boldsymbol{R_s}) \qquad (8)$$

$$\boldsymbol{FF_{SH}} = \boldsymbol{FF_o}(\mathbf{1} - \frac{\mathbf{1}}{\boldsymbol{R_{SH}}}) \qquad (9)$$

The series resistance was varied from 2Ω to 8Ω, and shunt resistance was varied from 10Ω to 40Ω. The effect of this variation is plotted in a contour-graph, as seen in figure 7.

It was seen that with the increase in series resistance the efficiency of the device was reduced to 4%, while with the increase in shunt resistance, the efficiency increased to 2% from 0.5%. From the theory mentioned above, the decrease in efficiency of the cell with series resistance can be attributed due to the increase in recombination probability, which reduces J_{sc}, and thereby, reducing the efficiency of the device. The high value of shunt resistance of the device helps to maintain a stable performance of the device as less current flows backwards across the p-n junction.

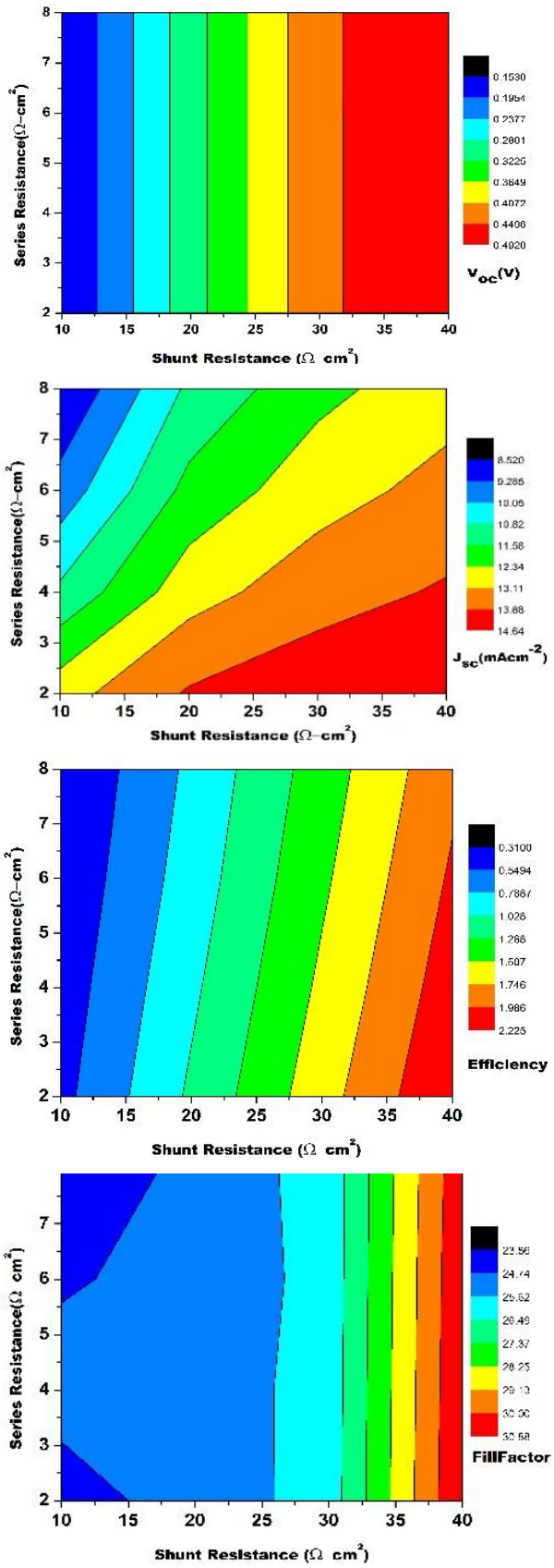

Figure 7. Contour plots showing variation of V_{oc}, J_{sc}, FF, and efficiency with series and shunt resistance.

Variation with temperature

To study the performance of the proposed device in the outside environment, a temperature variation study was carried out. The operating temperature was varied from 300 K to 500 K. As seen from the figure though, the current density remained at 15% the V_{oc}, FF, and efficiency declined from 0.541 V, 75.6%, and 6.54% at 300 K to 0.460679 V, 69.499%, and 4.9162% at 500 K. V_{oc} will get reduced due to the increase in reverse saturation current as per equation (10) [55].

$$V_{oc} = AV_{th}[\mathrm{LN}\left(1 + \frac{J_{sc}}{J_o}\right)] \quad 10$$

However, with the increase in temperature, the energy of the charge carriers also increases resulting in a higher percentage of recombination before reaching the depletion region, which results in a lower efficiency of the device, as seen from figure 8. This behaviour can also be recognized due to the increase in the interfacial defects with the rise in temperature, which increases the recombination or in other words, increases the series resistance, and thus decreases the efficiency.

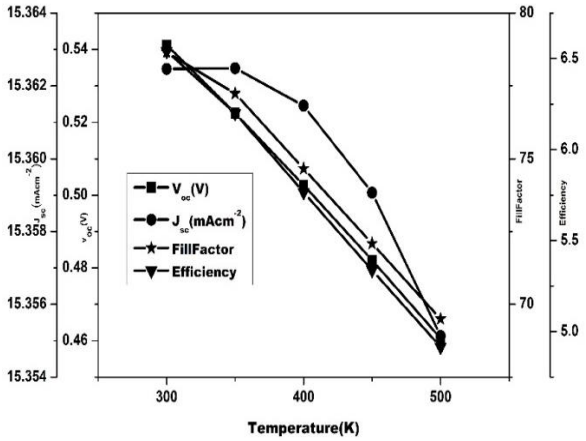

Figure 8. Effect of operating temperature on photovoltaic parameters of the device.

Electron affinity

The carrier recombination at the interfaces plays a major role in determining the efficiency of the device. The various layers must be carefully selected such that the recombination probability is as low as possible. This can be obtained by engineering there band offset of the absorber, HTL, and ETL. The Conduction Band Offset (CBO) and Valence Band Offset (VBO) can be optimized by using the following relations:

$$\mathbf{VBO = X_{HTL} - X_{PERV} + E_{GHTL} - E_{GPERV}}$$

$$\mathbf{CBO = \chi_{PERV} - \chi_{ETL}}$$

where χ_{PERV}, χ_{HTL}, and χ_{ETL} represent the electron affinities of the absorber [55], [56].

layer, HTL, and ETL, respectively. Also E_{gPERV} and E_{gHTL} represent the band gap of perovskite and ETL, respectively. Hence, by tuning the electron affinity of various layers, we can adjust CBO and VBO of the devices. In the present work, the electron affinity of the HTL layer and perovskite varied from 2 eV to 2.6 eV and 4 eV to 4.6 eV, respectively, as shown in figures 9(a) and 9(b). It can be seen that the electron affinity does not play any vital role in the various photovoltaic parameters of the device.

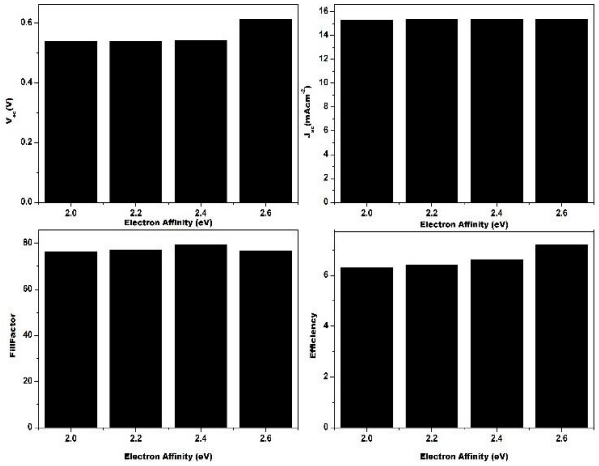

Figure 9(a). Effect on photovoltaic parameters due to variation in electron affinity of graphene oxide.

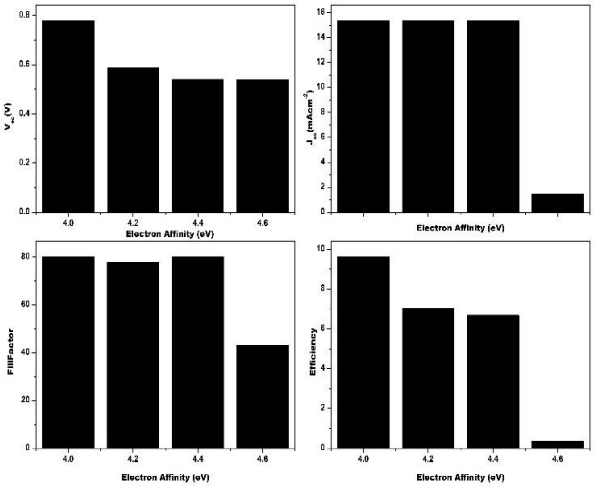

Figure 9(b). Effect on photovoltaic parameters due to variation in electron affinity of Cs_2TiBr_6 layer.

4. Conclusions

A simulation was carried out in the standard operating conditions for SCAPS-1D. The optimized thickness values for maximum PCE value were observed to be 1 μm for the absorber, 0.1 μm for HTL. The higher the thickness, the more the number of charge carriers formed but the higher will be the number of recombination of charge carriers too. The performance of the device

deteriorated when the defect density value increased for both interfaces, and it was found that the front interface density should be less than 10^{16} cm^{-3} and the back interface density less than 10^{10} cm^{-3} for an optimum performance. It can be attributed due to the larger number of recombinations at these interfaces. With the increase in the band gap, efficiency decreased from 15% to 3%, attributed to the lower photon absorption. The performance decreased with the increase in the operating temperature range, and the optimum temperature was found to be 300 K. Also the resistance values were fixed at 2Ω for series and 40Ω for shunt beyond, which it negatively affects the device performance. Finally, the electron affinity of the absorber seems to be not much involved with the inner working of the device as the parameters almost remained constant with a change in it. The elicited results suggest that Cs_2TiBr_6 can play a momentous role as an absorbing perovskite toward the highly efficient lead-free all-inorganic perovskite solar cell technology. The findings also reveal that GO could be a promising HTL for the fabrication of low-cost, high-efficiency caesium-based heterojunction solar cells. In short, the proposed structure has the potential to be a suitable substitute in developing highly efficient solar cells for photovoltaic applications after confirmation in the laboratory.

5. References

[1] Design and Simulation of Grid Connected Solar Si-Poly Photovoltaic Plant using PVsyst for Pune, India Location. Renewable Energy Research and Applications (RERA) Volume 3, Issue 1, January 2022, Pages 41-49, http://dx.doi.org/10.22044/rera.2021.11057.1069.

[2] Best Research-Cell Efficiency Chart, (n.d.). https://www.nrel.gov/pv/cell-efficiency.html (accessed June 12, 2022).

[3] J.D. Major, Grain boundaries in CdTe thin film solar cells: a review, Semicond. Sci. Technol. 31 (2016) 093001. https://doi.org/10.1088/0268-1242/31/9/093001.

[4] Colloidal Quantum Dot Solar Cells | Chemical Reviews, (n.d.). https://pubs.acs.org/doi/abs/10.1021/acs.chemrev.5b00063 (accessed June 12, 2022).

[5] Brief review of cadmium telluride-based photovoltaic technologies, (n.d.). https://www.spiedigitallibrary.org/journals/journal-of-photonics-for-energy/volume-4/issue-01/040996/Brief-review-of-cadmium-telluride-based-photovoltaic-technologies/10.1117/1.JPE.4.040996.full?SSO=1 (accessed June 12, 2022).

[6] Cracking perylene diimide backbone for fullerene-free polymer solar cells | Natalia Terenti-Academia.edu, (n.d.). https://www.academia.edu/35367843/Cracking_perylene_diimide_backbone_for_fullerene-free_polymer_solar_cells (accessed June 12, 2022).

[7] J.H. Noh, S.H. Im, J.H. Heo, T.N. Mandal, and S.I. Seok, Chemical Management for Colorful, Efficient, and Stable Inorganic–Organic Hybrid Nanostructured Solar Cells, Nano Lett. 13 (2013) 1764–1769. https://doi.org/10.1021/nl400349b.

[8] S. De Wolf, J. Holovsky, S.-J. Moon, P. Löper, B. Niesen, M. Ledinsky, F.-J. Haug, J.-H. Yum, and C. Ballif, Organometallic Halide Perovskites: Sharp Optical Absorption Edge and its Relation to Photovoltaic Performance, J Phys Chem Lett. 5 (2014) 1035–1039. https://doi.org/10.1021/jz500279b.

[9] S. Prasanthkumar and L. Giribabu, Recent Advances in Perovskite-Based Solar Cells, Current Science. 111 (2016) 1173–1181. https://doi.org/10.18520/cs/v111/i7/1173-1181.

[10] Electron-Hole Diffusion Lengths Exceeding 1 Micrometer in an Organometal Trihalide Perovskite Absorber, (n.d.). https://www.science.org/doi/10.1126/science.1243982 (accessed June 12, 2022).

[11] A. Kojima, K. Teshima, and Y. Shirai, T. Miyasaka, Organometal Halide Perovskites as Visible-Light Sensitizers for Photovoltaic Cells, J. Am. Chem. Soc. 131 (2009) 6050–6051. https://doi.org/10.1021/ja809598r.

[12] D. Liu and T.L. Kelly, Perovskite solar cells with a planar heterojunction structure prepared using room-temperature solution processing techniques, Nature Photonics. 8 (2014) 133–138. https://doi.org/10.1038/nphoton.2013.342.

[13] Viability of Lead-Free Perovskites with Mixed Chalcogen and Halogen Anions for Photovoltaic Applications | The Journal of Physical Chemistry C, (n.d.). https://pubs.acs.org/doi/abs/10.1021/acs.jpcc.6b00920 (accessed June 12, 2022).

[14] Thin-Film Deposition and Characterization of a Sn-Deficient Perovskite Derivative Cs2SnI6 | Chemistry of Materials, (n.d.). https://pubs.acs.org/doi/abs/10.1021/acs.chemmater.6b00433 (accessed June 12, 2022).

[15] Searching for promising new perovskite-based photovoltaic absorbers: the importance of electronic dimensionality-Materials Horizons (RSC Publishing), (n.d.). https://pubs.rsc.org/en/content/articlelanding/2017/mh/c6mh00519e (accessed June 12, 2022).

[16] Engineering Interface Structure to Improve Efficiency and Stability of Organometal Halide Perovskite Solar Cells | The Journal of Physical

Chemistry B, (n.d.). https://pubs.acs.org/doi/10.1021/acs.jpcb.7b03921 (accessed June 12, 2022).

[17] Light-induced reactivity of gold and hybrid perovskite as a new possible degradation mechanism in perovskite solar cells-Journal of Materials Chemistry A (RSC Publishing), (n.d.). https://pubs.rsc.org/en/content/articlelanding/2018/ta/c7ta10217h (accessed June 12, 2022).

[18] High-Performance Formamidinium-based Perovskite Solar Cells via Microstructure-Mediated δ-to-α Phase Transformation | Chemistry of Materials, (n.d.). https://pubs.acs.org/doi/10.1021/acs.chemmater.7b00523 (accessed June 12, 2022).

[19] P. Qin, S. Tanaka, S. Ito, N. Tetreault, K. Manabe, H. Nishino, M.K. Nazeeruddin, and M. Grätzel, Inorganic hole conductor-based lead halide perovskite solar cells with 12.4% conversion efficiency, Nat Commun. 5 (2014) 3834. https://doi.org/10.1038/ncomms4834.

[20] E. Mosconi, P. Umari, and F.D. Angelis, Electronic and optical properties of mixed Sn–Pb organohalide perovskites: a first principles investigation, J. Mater. Chem. A. 3 (2015) 9208–9215. https://doi.org/10.1039/C4TA06230B.

[21] Anomalous Band Gap Behavior in Mixed Sn and Pb Perovskites Enables Broadening of Absorption Spectrum in Solar Cells | Journal of the American Chemical Society, (n.d.). https://pubs.acs.org/doi/10.1021/ja5033259 (accessed June 12, 2022).

[22] T. Krishnamoorthy, H. Ding, C. Yan, W.L. Leong, T. Baikie, Z. Zhang, M. Sherburne, S. Li, M. Asta, N. Mathews, and S.G. Mhaisalkar, Lead-free germanium iodide perovskite materials for photovoltaic applications, J. Mater. Chem. A. 3 (2015) 23829–23832. https://doi.org/10.1039/C5TA05741H.

[23] G. Niu, H. Yu, J. Li, D. Wang, and L. Wang, Controlled orientation of perovskite films through mixed cations toward high performance perovskite solar cells, Nano Energy. 27 (2016) 87–94. https://doi.org/10.1016/j.nanoen.2016.06.053.

[24] Enhancement of thermal stability for perovskite solar cells through cesium doping-RSC Advances (RSC Publishing), (n.d.). https://pubs.rsc.org/en/content/articlelanding/2017/ra/c6ra28501e (accessed June 12, 2022).

[25] Enhanced Charge Carrier Transport and Device Performance Through Dual-Cesium Doping in Mixed-Cation Perovskite Solar Cells with Near Unity Free Carrier Ratios | ACS Applied Materials & Interfaces, (n.d.). https://pubs.acs.org/doi/abs/10.1021/acsami.6b12845 (accessed June 14, 2022).

[26] Die Gesetze der Krystallochemie | SpringerLink, (n.d.). https://link.springer.com/article/10.1007/BF01507527 (accessed June 12, 2022).

[27] Stabilizing Perovskite Structures by Tuning Tolerance Factor: Formation of Formamidinium and Cesium Lead Iodide Solid-State Alloys | Chemistry of Materials, (n.d.). https://pubs.acs.org/doi/10.1021/acs.chemmater.5b04107 (accessed June 12, 2022).

[28] T. Saha-Dasgupta, Double perovskites with 3d and 4d/5d transition metals: compounds with promises, Mater. Res. Express. 7 (2020) 014003. https://doi.org/10.1088/2053-1591/ab6293.

[29] Earth-Abundant Nontoxic Titanium(IV)-based Vacancy-Ordered Double Perovskite Halides with Tunable 1.0 to 1.8 eV Bandgaps for Photovoltaic Applications | ACS Energy Letters, (n.d.). https://pubs.acs.org/doi/10.1021/acsenergylett.7b01167 (accessed June 12, 2022).

[30] D. Kong, D. Cheng, X. Wang, K. Zhang, H. Wang, K. Liu, H. Li, X. Sheng, and L. Yin, Solution processed lead-free cesium titanium halide perovskites and their structural, thermal and optical characteristics, J. Mater. Chem. C. 8 (2020) 1591–1597. https://doi.org/10.1039/C9TC05711K.

[31] M. Chen, M.-G. Ju, A.D. Carl, Y. Zong, R.L. Grimm, J. Gu, X.C. Zeng, Y. Zhou, and N.P. Padture, Cesium Titanium(IV) Bromide Thin Films based Stable Lead-free Perovskite Solar Cells, Joule. 2 (2018) 558–570. https://doi.org/10.1016/j.joule.2018.01.009.

[32] Improved stability and efficiency of perovskite solar cells with submicron flexible barrier films deposited in air-Journal of Materials Chemistry A (RSC Publishing), (n.d.). https://pubs.rsc.org/en/content/articlelanding/2017/ta/c7ta09178h (accessed June 12, 2022).

[33] Highly reproducible perovskite solar cells based on solution coating from mixed solvents - Document-Gale Academic OneFile, (n.d.). https://go.gale.com/ps/i.do?id=GALE%7CA518490884&sid=googleScholar&v=2.1&it=r&linkaccess=abs&issn=00222461&p=AONE&sw=w&userGroupName=anon%7Ebc86b822 (accessed June 12, 2022).

[34] A. Dubey, N. Adhikari, S. Mabrouk, F. Wu, K. Chen, S. Yang, and Q. Qiao, A strategic review on processing routes towards highly efficient perovskite solar cells, J. Mater. Chem. A. 6 (2018) 2406–2431. https://doi.org/10.1039/C7TA08277K.

[35] A. Fakharuddin, L. Schmidt-Mende, G. Garcia-Belmonte, R. Jose, and I. Mora-Sero, Interfaces in Perovskite Solar Cells, Advanced Energy Materials. 7 (2017) 1700623. https://doi.org/10.1002/aenm.201700623.

[36] M.A. Nalianya, C. Awino, H. Barasa, V. Odari, F. Gaitho, B. Omogo, and M. Mageto, Numerical study of

lead free CsSn0.5Ge0.5I3 perovskite solar cell by SCAPS-1D, Optik. 248 (2021) 168060. https://doi.org/10.1016/j.ijleo.2021.168060.

[37] D.K. Jarwal, A.K. Mishra, A. Kumar, S. Ratan, A.P. Singh, C. Kumar, B. Mukherjee, and S. Jit, Fabrication and TCAD simulation of TiO_2 nanorods electron transport layer based perovskite solar cells, Superlattices and Microstructures. 140 (2020) 106463. https://doi.org/10.1016/j.spmi.2020.106463.

[38] S. Hosseini, M. Bahramgour, N. Delibaş, and A. Niaie, Investigation of a Perovskite Solar Cell and Various Parameters Impact on Its Layers and the Effect of Interface Modification by Using P3HT as an Ultrathin Polymeric Layer Through SCAPS-1D Simulation, Sakarya University Journal of Science. 25 (2021) 1168–1179. https://doi.org/10.16984/saufenbilder.947735.

[39] J.-Y. Jeng, Y.-F. Chiang, M.-H. Lee, S.-R. Peng, T.-F. Guo, P. Chen, and T.-C. Wen, CH3NH3PbI3 Perovskite/Fullerene Planar-Heterojunction Hybrid Solar Cells, Advanced Materials. 25 (2013) 3727–3732. https://doi.org/10.1002/adma.201301327.

[40] Novel graphene-based transparent electrodes for perovskite solar cells-Iqbal-2018- International Journal of Energy Research-Wiley Online Library, (n.d.). https://onlinelibrary.wiley.com/doi/abs/10.1002/er.4244 (accessed June 12, 2022).

[41] Low temperature processed inverted planar perovskite solar cells by r-GO/CuSCN hole-transport bilayer with improved stability | Semantic Scholar, (n.d.). https://www.semanticscholar.org/paper/Low-temperature-processed-inverted-planar-solar-by-Chowdhury-Akhtaruzzaman/1989e25a31cf265aff03fcacc752607851780b70 (accessed June 12, 2022).

[42] Reduced Graphene Oxide as a Stabilizing Agent in Perovskite Solar Cells-Milić-2018- Advanced Materials Interfaces-Wiley Online Library, (n.d.). https://onlinelibrary.wiley.com/doi/abs/10.1002/admi.201800416 (accessed June 12, 2022).

[43] MoS_2 Quantum Dot/Graphene Hybrids for Advanced Interface Engineering of a $CH_3NH_3PbI_3$ Perovskite Solar Cell with an Efficiency of over 20% | ACS Nano, (n.d.). https://pubs.acs.org/doi/abs/10.1021/acsnano.8b05514 (accessed June 12, 2022).

[44] Z. Zhu, J. Ma, Z. Wang, C. Mu, Z. Fan, L. Du, Y. Bai, L. Fan, H. Yan, D.L. Phillips, and S. Yang, Efficiency enhancement of perovskite solar cells through fast electron extraction: the role of graphene quantum dots, J Am Chem Soc. 136 (2014) 3760–3763. https://doi.org/10.1021/ja4132246.

[45] A numerical study of high efficiency ultra-thin CdS/CIGS solar cells: African Journal of Science, Technology, Innovation and Development: Vol. 8, No. 4, (n.d.). https://www.tandfonline.com/doi/abs/10.1080/20421338.2015.1118929 (accessed June 13, 2022).

[46] Modeling thin-film PV devices-Burgelman-2004-Progress in Photovoltaics: Research and Applications-Wiley Online Library, (n.d.). https://onlinelibrary.wiley.com/doi/10.1002/pip.524 (accessed June 13, 2022).

[47] M. Mostefaoui, H. Mazari, S. Khelifi, A. Bouraiou, and R. Dabou, Simulation of High Efficiency CIGS Solar Cells with SCAPS-1D Software, Energy Procedia. 74 (2015) 736–744. https://doi.org/10.1016/j.egypro.2015.07.809.

[48] R.T. Mouchou, T.C. Jen, O.T. Laseinde, and K.O. Ukoba, Numerical simulation and optimization of p-NiO/n-TiO2 solar cell system using SCAPS, Materials Today: Proceedings. 38 (2021) 835–841. https://doi.org/10.1016/j.matpr.2020.04.880.

[49] A. Slami, M. Bouchaour, and L. Merad, Numerical Study of Based Perovskite Solar Cells by SCAPS-1D, INTERNATIONAL JOURNAL OF ENERGY and ENVIRONMENT. 13 (2019) 5.

[50] Numerical development of eco-friendly Cs2TiBr6 based perovskite solar cell with all-inorganic charge transport materials via SCAPS-1D - ScienceDirect, (n.d.). https://www.sciencedirect.com/science/article/abs/pii/S0030402620315916 (accessed June 13, 2022).

[51] E. Widianto, E. Subama, N.M. Nursam, K. Triyana, and I. Santoso, Design and simulation of perovskite solar cell using graphene oxide as hole transport material, AIP Conference Proceedings. 2391 (2022) 090011. https://doi.org/10.1063/5.0073007.

[52] S.S. Mali and C.K. Hong, p-i-n/n-i-p type planar hybrid structure of highly efficient perovskite solar cells towards improved air stability: synthetic strategies and the role of p-type hole transport layer (HTL) and n-type electron transport layer (ETL) metal oxides, Nanoscale. 8 (2016) 10528–10540. https://doi.org/10.1039/C6NR02276F.

[53] N. Jensen, R.M. Hausner, R.B. Bergmann, J.H. Werner, and U. Rau, Optimization and characterization of amorphous/crystalline silicon heterojunction solar cells, Progress in Photovoltaics: Research and Applications. 10 (2002) 1–13. https://doi.org/10.1002/pip.398.

[54] Enhancing the open circuit voltage of the SnS based heterojunction solar cell using NiO HTL | Semantic Scholar, (n.d.). https://www.semanticscholar.org/paper/Enhancing-the-open-circuit-voltage-of-the-SnS-based-Ahmmed-Aktar/3ae20147f81aa5b95fc84216bc4a5bd37dfd5468 (accessed June 14, 2022).

[55] Investigating the performance of formamidinium tin-based perovskite solar cell by SCAPS device simulation - NASA/ADS, (n.d.).

https://ui.adsabs.harvard.edu/abs/2020OptMa.101097 38A/abstract (accessed June 13, 2022).

[56] Evidence of improved power conversion efficiency in lead-free CsGeI3 based perovskite solar cell heterostructure via scaps simulation: Journal of Vacuum Science & Technology B: Vol. 39, No. 1, (n.d.). https://avs.scitation.org/doi/10.1116/6.0000718 (accessed June 13, 2022).